Mineralogical Magazine (2022), **86**, 570–576
doi:10.1180/mgm.2022.41

CAMBRIDGE UNIVERSITY PRESS

Article

Special Issue dedicated to Peter Williams

Bridgesite-(Ce), a new rare earth element sulfate, with a unique crystal structure, from Tynebottom Mine, Cumbria, United Kingdom

Mike S. Rumsey[1]*, Frank C. Hawthorne[2], John Spratt[3], Jens Najorka[3] and Wren Montgomery[3]

[1]Mineral and Planetary Science Collections, Department of Science, Natural History Museum, Cromwell Road, London SW7 5BD, United Kingdom; [2]Department of Geological Sciences, University of Manitoba, Winnipeg, Manitoba R3T 2N2, Canada; and [3]Core Research Laboratories, Department of Science, Natural History Museum, Cromwell Road, London SW7 5BD, United Kingdom

Abstract

Bridgesite-(Ce), (IMA2019-034), was discovered at Tynebottom Mine, Cumbria, UK. It occurs as thin (1–2 μm) translucent blue crystals with a lath-like to acicular habit, aggregated into thin crusts and is associated mainly with brochantite, malachite, serpierite, devilline, gypsum, aragonite, jarosite, pyrite, lanthanite-(Ce) and undifferentiated iron oxyhydroxides, it is often intergrown with these other minerals. The lustre, hardness, cleavage and parting could not be determined, nor could density be measured due to crystal size. It has a pale blue streak and is brittle with a splintery fracture. Bridgesite-(Ce) is biaxial (–), shows no pleochroism and has refractive indices (white light): $\alpha = 1.526(2)$, $\beta = 1.564(2)$, $\gamma = 1.572(2)$ and $2V_{(calc)} = 48.3°$. The empirical formula calculated on the basis of 44 negative charges is $Ca_{0.86}REE_{\Sigma 1.99}Al_{0.07}Cu_{5.95}(SO_4)_{3.99}(SiO_4)_{0.05}(PO_4)_{0.02}(OH)_{11.52}{\cdot}8H_2O$. The idealised formula is $CaCe_2Cu_6(SO_4)_4(OH)_{12}{\cdot}8H_2O$, requiring (wt.%): 3.91 CaO, 22.89 Ce_2O_3, 33.28 CuO, 22.33 SO_3 and 17.59 H_2O. Bridgesite-(Ce) is monoclinic, space group C2/m, $a =$ 24.801(5), $b = 6.3520(13)$, $c = 11.245(2)$ Å, $\beta = 114.51(3)°$, $V = 1611.9(6)$ Å and $Z = 2$. The five most intense X-ray diffraction peaks in the measured pattern are [*d* in Å (*I*, %) (*hkl*)]: 11.3 (100) (200), 6.391 (15) (201), 2.770 (8) (420), 3.194 (6) (402) and 4.858 (5) (310). The crystal structure was solved using single crystal data and refined to an R_1 index of 5.86%. Bridgesite-(Ce) contains three distinct Cu sites containing Cu^{2+}, two are coordinated octahedrally and one is square pyramidal. The octahedra form chains through edge sharing parallel to the b-axis which are linked by the square pyramid to form sheets oriented parallel to {100}. Sulfate tetrahedra decorate the sheets which are held together by interstitial REE^{3+}, Ca^{2+} and hydrogen bonding. The structure is unique. Despite apparent similarity in chemical formula, bridgesite-(Ce) is not closely related to any other natural Cu-sulfate mineral. An FTIR absorption spectra is presented for reference purposes.

Keywords: new mineral, unique element combination, crystal structure, cerium, REE, United Kingdom, Tynebottom, post mining, anthropocene

(Received 19 June 2019; accepted 15 April 2022; Accepted Manuscript published online: 27 April 2022; Associate Editor: G. Diego Gatta)

Introduction

Bridgesite-(Ce) is a new supergene mineral, found sparingly with other sulfates, on a pile of post-mining waste rock in the Dryburn Washpool flats of Tynebottom Mine, Garrigill, Cumbria, UK (54° 46′16″N, 2°24′26″W). The mine worked the veins and replacement flats in the Tynebottom Limestone (Brigantian) for lead and zinc as early as 1771 (Dunham, 1948) but has been abandoned for many years. It is well known to mineral collectors for Co-bearing secondary minerals. Parts of the mine are still accessible and used for outdoor pursuits. It is notified as a Site of Special Scientific Interest (SSSI) and collecting is managed through the non-departmental public body, Natural England.

The specimens of bridgesite-(Ce) in this study were collected in 1983. Specimens were relatively common at the time, but the occurrence has since been almost completely removed. Subsequent investigation of the collections at the Natural History Museum (NHM), London uncovered more material from what is probably the same occurrence, the earliest dating to 1950. Bridgesite-(Ce) is also present on a specimen labelled as brochantite, that was collected in 1979 (BM 1979,458). During final preparation of this manuscript and after publication in the newsletter of the Commission on New Minerals, Nomenclature and Classification of the International Mineralogical Association (IMA-CNMNC, Rumsey *et al.*, 2019) it has become clear that there are further specimens collected at various times lodged in private topographical collections in the UK.

Bridgesite-(Ce), phonetically [brɪˈdʒɪz.aɪt], is named in honour of Trevor Bridges (1935–2015), professional chemist, amateur geologist, mineral collector, mountaineer, munroist, founding member of the Russell Society's northern branch in 1984, and author of many papers regarding mineralogy and geochemistry in the British Isles. Trevor identified the potential for a new mineral and mentioned it in his study of the supergene mineralisation

***Author for correspondence:** Mike S. Rumsey, Email: m.rumsey@nhm.ac.uk
This paper is part of a thematic set that honours the contributions of Peter Williams
Cite this article: Rumsey M.S., Hawthorne F.C., Spratt J., Najorka J. and Montgomery W. (2022) Bridgesite-(Ce), a new rare earth element sulfate, with a unique crystal structure, from Tynebottom Mine, Cumbria, United Kingdom. *Mineralogical Magazine* **86**, 570–576. https://doi.org/10.1180/mgm.2022.41

at Tynebottom (Bridges and Green, 2007). It is for Trevor's long standing and significant contribution to British mineralogy and as the collector of the samples used in this study that he is honoured with its name. The new mineral and name (symbol Bdg-Ce) were approved by the Commission of New Minerals, Nomenclature and Classification (IMA2019-034, Rumsey *et al.*, 2019).

Although, the holotype sample was submitted for identification at the NHM in 1983 it has the more recent registration number BM 2007,81. All characterisation relevant chemical and structural data were obtained from sub-samples taken from this specimen. Further, newly available specimens were used to obtain a powder diffraction pattern and an infrared spectrum for reference purposes. The acquisition of more samples is ongoing and author-designated cotypes in addition to those at the NHM (BM 2007,82 and BM 2007,83) will be provided to other institutions for safe keeping.

Occurrence

The waste-rock pile on which bridgesite-(Ce) was found contains dark, recrystallised limestone with millimetre-sized blebs of pyrite, chalcopyrite and rare galena; it is very similar to the limestone in the walls of the mine where the pile is sited, and the rocks do not appear to have moved far from their original location. On the limestone, bridgesite-(Ce) occurs with other sulfates as crusts which are separated into bands. The associated minerals found to date include brochantite, malachite, serpierite, devilline, linarite, wroewolfeite, gypsum, cerussite, aragonite, jarosite, brianyoungite, lanthanite-(Ce), agardite-(*REE*), pyrite, chalcopyrite, galena, hydrozincite and undifferentiated iron oxyhydroxides.

The origin of the supergene assemblage has been studied in detail by Bridges and Green (2007) who suggest that it is the product of water percolating through the sulfide-bearing orebodies and dripping onto waste limestone rock in a humid mine environment. This interaction produces acid solutions rich in dissolved sulfate and metal ions (Cu, Fe, Zn and Pb) that precipitate supergene minerals as the water evaporates. The banding is a consequence of differential precipitation, different supergene minerals dominating in different regions because of the gradual increase in pH and change in chemistry as fluid migrates from where it drips onto the pile as it is neutralised by the host limestone. The rare earth elements (REE) may come from the breakdown of a calcium–cerium mineral, assumed to be synchysite-(Ce), which has been reported as a constituent of the first phase of mineralisation at the mine (Ixer and Stanley, 1987) or from other REE minerals which are known to be present in the orefield (Ixer, 2003). Although, like many supergene minerals, anthropogenic activity has clearly had an influence in creating the environment in which bridgesite-(Ce) was found (on broken waste rock in an adit), entirely geological occurrences of the mineral are not unlikely given the right chemical and environmental conditions.

Physical and optical properties

Bridgesite-(Ce) occurs on the holotype specimen, and all other identified specimens as small tufts and patches of teal/sky-blue [HTML: 3BB9FF] needle-like crystals, very similar in appearance to serpierite (Fig. 1). Individual crystals are generally ~200 μm in length, 10–20 μm in width and 1–2 μm thick (Fig. 2). The thin, elongate crystals regularly grow with a radial almost acicular habit. Scanning electron microscopy images show different forms, including chisel-like and pointed terminations. Small

Fig. 1. Close-up of acicular bridgesite-(Ce) crystals on cotype sample BM 2007,82. The scale bar is 200 μm and the associated colourless crystal to the bottom left is gypsum.

regions of steeply terminated, acicular 'feathery' crystals intergrown with bridgesite-(Ce) have the same major-element composition when analysed using semi-quantitative energy-dispersive X-ray analysis methods but may ultimately not be equivalent. The lustre, hardness, cleavage, and parting of bridgesite-(Ce) could not be assessed nor could the density be measured due to the small crystal size. The mineral is non-fluorescent, has a pale-blue streak, is translucent and brittle with a splintery fracture, slightly curved crystals may indicate minor flexibility. The density calculated using the empirical formula and crystal structure is 2.847 g/cm^3.

A number of larger bridgesite-(Ce) grains selected for optical study did not extinguish properly (and are therefore polycrystalline), so the very small (2 μm × 7 μm × 50 μm) crystal selected for single-crystal X-ray diffraction was also used for optics. The optic axial angle was measured with a spindle stage using the program *Excalibr2* (Bartelmehs *et al.*, 1992). Bridgesite-(Ce) is biaxial (–), with $\alpha = 1.526(2)$, $\beta = 1.564(2)$ and $\gamma = 1.572(2)$, measured in white light with $2V_{(meas)} = 53.0(10)°$ and $2V_{(calc)} = 48.3°$. It is non-pleochroic.

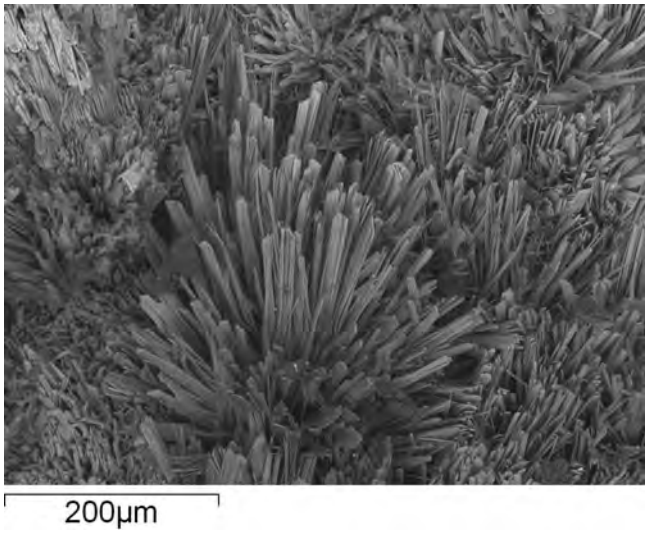

Fig. 2. Bridgesite-(Ce) in lath-like acicular crusts to 0.2 mm. Note the variation in crystal terminations and the splintery fracture (holotype BM 2007,81).

Chemical composition

The thickness and elongated habit of the crystals made acquisition of chemical data challenging. Over 100 analyses were obtained on two separate occasions, using a Cameca SX100 electron microprobe in wave-length dispersive mode operating at 20 kV, 20 nA and a spot size of 5 μm at the NHM in London.

Both datasets are similar, with chemical signatures dominated by Cu, Ca, *REE*, S and low totals, suggesting the presence of significant H_2O. Across both datasets, the elements Na, Mg, Al, Si, Ca, Cu, P, Cl, Ce, La, Y, Nd, Gd, Dy, Pr, Sm, Fe, Eu and Sr were sought; Na, Mg, Fe and Sr were below detection limits. The most complete dataset was used in the calculation of the empirical formula.

The excitation volume of the electron beam is undoubtedly larger than the target bridgesite-(Ce) crystals which are only 1–2 μm thick. Therefore, small variations in the dominant elements are interpreted as contributions from contaminant phases, most commonly brochantite and lanthanite-(Ce). These contributions were removed by discarding any data point with one of the dominant element analyses outside of 1.5 standard deviations from its median value.

The remaining dataset ($n = 16$) from the holotype sample, BM 2007,81, is summarised in Table 1; standard deviations are based on this dataset only. Water and carbonate could not be determined directly due to the small amount of material available and the inability to separate pure fragments of a suitable size. Therefore H_2O was calculated on the basis of the single-crystal X-ray study which did not reveal the presence of any carbonate.

The variability and low average analytical total is also interpreted as an effect of the mismatch between the electron-beam excitation-volume and crystals studied. An additional factor may be the lack of data on the heavy REE (Tb, Eu, Ho, Er, Tm, Yb and Lu), though these elements typically make up a relatively small fraction of total REE contents. The propensity of hydrous minerals like bridgesite-(Ce) to dehydrate under the electron beam may also have contributed specifically to variability.

The empirical formula, using the data in Table 1, calculated on the basis of 44 negative charges, the crystallographic study, and including silicon as silicate, phosphorus as phosphate and aluminium as Al^{3+} is $Ca_{0.86}REE_{\Sigma 1.99}Al_{0.07}Cu_{5.95}(SO_4)_{3.99}(SiO_4)_{0.05}(PO_4)_{0.02}(OH)_{11.52}\cdot 8H_2O$. This suggests an ideal formula $CaCe_2Cu_6(SO_4)_4(OH)_{12}\cdot 8H_2O$, which requires (wt.%): 3.91 CaO, 22.89 Ce_2O_3, 33.28 CuO, 22.33 SO_3 and 17.59 H_2O.

Bridgesite-(Ce) is somewhat enriched in light REE compared to chondrite normalised values and to the trace-element composition of fluorite from the North Pennine Orefield but is depleted in yttrium and the heavy REE gadolinium and dysprosium.

The Gladstone-Dale compatibility index for the empirical formula is –0.005, which is superior (Mandarino, 2007).

Table 1. Chemical data (in wt %) for bridgesite-(Ce).

Constituent	Mean	Range	S.D.	Reference material
SiO_2	0.21	0.08–0.41	0.09	Fayalite
Al_2O_3	0.23	0.02–0.75	0.24	Corundum
P_2O_5	0.10	b.d–0.19	0.06	$ScPO_4$
SO_3	21.83	16.25–24.38	2.58	Celestine
CaO	3.28	2.82–3.83	0.29	Wollastonite
CuO	32.36	27.31–37.44	2.61	Cu metal
La_2O_3	2.92	2.37–3.47	0.34	La glass
Ce_2O_3	8.66	7.19–9.78	0.74	Ce glass
Y_2O_3	0.59	0.40–0.79	0.11	Y glass
Pr_2O_3	1.27	0.99–1.50	0.14	Pr glass
Nd_2O_3	6.11	4.63–7.07	0.70	Nd glass
Sm_2O_3	1.48	1.23–1.88	0.20	Sm glass
Gd_2O_3	1.18	0.88–1.48	0.17	Gd glass
Dy_2O_3	0.30	0.21–0.38	0.06	Dy glass
ΣREE_2O_3	22.52	18.30–25.68	2.06	N/A
$H_2O_{(calc)}$	17.28			
Total	97.80			

b.d. – below detection; S.D. – standard deviation

Crystal structure solution and refinement

A single-crystal fragment of bridgesite-(Ce) from the holotype specimen was attached to a tapered glass fibre and mounted on a Bruker APEX II ULTRA three-circle diffractometer equipped with a rotating-anode generator (Mo*K*α), multilayer optics and an APEX II 4K CCD detector. A total of 20,306 intensities was collected to $2\theta = 50°$ using 120 s per 0.3° frame with a crystal-to-detector distance of 5 cm (diffracted intensities are extremely weak; the crystal measured 2 μm × 7 μm × 50 μm). Empirical absorption corrections (*SADABS*; Sheldrick, 2008) were applied and equivalent reflections were merged, resulting in 1597 unique reflections. The unit-cell dimensions were obtained by least-squares refinement of the positions of 3254 reflections with $I > 10\sigma I$. The crystal structure of bridgesite-(Ce) was solved by direct methods and refined in the space group *C*2/*m* to an R_1 index of 5.86%. Attempts to refine the structure of bridgesite-(Ce) in lower symmetry (*C*2 and *Cm*) were unsuccessful; In both lower-symmetry space groups the refinements were unstable, characterised by highly unrealistic displacement parameters for atom pairs equivalent in *C*2/*m*. Moreover, the refinements would not converge properly. Except for the partly occupied H_2O sites, the *C*2/*m* structure is well-ordered and shows no sign of deviation from *C*2/*m* symmetry. Miscellaneous data are summarised in Table 2, atom positions and equivalent-isotropic displacement parameters are given in Table 3 and selected interatomic distances in Table 4. The crystallographic information file has been deposited with the Principal Editor of *Mineralogical Magazine* and is available as Supplementary material (see below).

Table 2. Miscellaneous information for bridgesite-(Ce).

Crystal data	
Crystal size (μm)	2 × 7 × 50
a (Å)	24.081(5)
b	6.3520(13)
c	11.245(2)
β (°)	114.51(3)
V (Å^3)	1161.9(6)
Z	4
a : *b* : *c*	3.7911 : 1 : 1.7703
Space group	*C*2/*m*
Data collection and refinement	
Unit cell reflections	3254 > 10σ*I*
Total reflections	20,306
Ewald reflections	1626
Unique reflections	1597
No. with $F_o > 4\sigma F$	1182
R_{merge} %	8.87
R_1 %	5.86
wR_2 %	16.75
A, B weights	0.1162, 54.69
2θ limit (°)	50
D_{calc} (g/cm^3)	2.847

Table 3. Atom coordinates for bridgesite-(Ce).

Atom	*x*	*y*	*z*	U_{eq}
Ce	0.32313(5)	0	0.30131(9)	0.0225(4)
*Cu*1	0.27732(10)	–½	0.2969(2)	0.0218(5)
*Cu*2	¼	–¾	½	0.0238(6)
*Cu*3	¼	¼	0	0.0198(6)
*S*1	0.1307(3)	–½	0.2095(5)	0.059(2)
*S*2	0.3824(2)	–½	0.2037(5)	0.0333(12)
Ca	0.4377(3)	–½	–0.0013(7)	0.025(2)
O1	0.2474(4)	0.2639(13)	0.1718(7)	0.020(2)
O2	0.3109(4)	0.2836(14)	0.4345(8)	0.027(1)
O3	0.3003(5)	0	0.0627(10)	0.020(3)
O4	0.1867(5)	–½	0.3228(12)	0.027(3)
O5	0.2277(6)	–1.0	0.3889(11)	0.029(3)
O6	0.4153(6)	0	0.5102(13)	0.038(3)
O7	0.0818(6)	–½	0.2467(13)	0.044(4)
O8	0.4120(8)	½	0.603(2)	0.062(5)
O9	0.3402(8)	–½	0.0671(13)	0.055(5)
O10	0.4421(8)	–½	0.215(2)	0.074(6)
O11	0.3743(8)	–0.684(3)	0.2704(12)	0.130(9)
O12	0.1279(6)	–0.695(5)	0.137(2)	0.23(2)
O13	0.4716(11)	–0.865(4)	0.080(2)	0.071(10)
O14	0.427(2)	0	0.271(4)	0.04*
O15	1.2	–0.295(4)	½	0.04*

*Fixed during refinement.

Powder X-ray diffraction pattern

As there was not enough material on the holotype for powder diffraction, a small polycrystalline fragment from a different specimen was attached to a carbon fibre, mounted on a Rigaku D-max Rapid II at 40 Kv and 36 mA, and analysed using Gandolfi-type movements. The measured peak positions fit the unit cell determined by singe-crystal diffraction and are presented in Table 5. The 200 (*hkl*) peak, which has elevated intensity relative to the calculated pattern is interpreted as a preferred orientation effect.

Structure description

Bridgesite-(Ce) contains three *Cu* sites containing Cu^{2+}. Cu(1) is [5]-coordinated by one O^{2-} ion and four $(OH)^{-}$ ions arranged in a square pyramid (Fig. 3a) with a <Cu(1)–O> distance of 2.060 Å. Cu(2) and Cu(3) are each [6]-coordinated by two O^{2-} ions and four $(OH)^{-}$ ions in octahedral arrangements (Fig. 3b,c) with <Cu(2)–O> and <Cu(3)–O> distances of 2.138 and 2.169 Å, respectively (Table 3, Fig. 3a), reasonably close to the grand $<^{[6]}Cu^{2+}–O>$ distances of 2.150 Å given for $^{[6]}Cu^{2+}$-oxysalt minerals by Burns and Hawthorne (1996) and well within the range of $<^{[6]}Cu^{2+}–O>$ distances given by Eby and Hawthorne (1993): 2.08–2.35 Å. There are two S sites occupied by S^{6+}, each of which is tetrahedrally coordinated by four O^{2-} anions with <S–O> distances of 1.464 and 1.453 Å, respectively (Table 4 and Fig. 4a), somewhat smaller than the grand mean value of 1.473 Å for both sulfate minerals (Hawthorne *et al.*, 2000) and inorganic sulfate structures (Gagné and Hawthorne, 2018). There is one *Ce* site occupied dominantly by Ce^{3+} and coordinated by three O^{2-} ions, six $(OH)^{-}$ ions and one (H_2O) group (Fig. 3d) with a $<Ce^{3+}–O>$ distance of 2.576 Å, close to the grand $<Ce^{3+}–O>$ distance of 2.553 Å given for inorganic Ce^{3+}-bearing structures by Gagné (2018). There is one *Ca* site half-occupied by Ca^{2+} and coordinated by four O^{2-} ions and two $(OH)^{-}$ ions with a <*Ca*–O> distance of 2.56 Å (Table 3, Fig. 3e).

The bond-valence table (Table 6) shows that O4, O7, O9, O10, O11 and O12 have incident bond-valence sums close to 2 valence units (vu) and hence are O^{2-} ions (as required by the valence-sum rule). O1, O2, O3 and O5 have incident bond-valence sums close to 1 vu and hence are OH ions as no F or Cl was detected in the electron microprobe analyses (Brown 2016, Hawthorne 2012, 2015). O6, O8, O13, O14 and O15 have incident bond-valence sums close to 0 vu and hence are (H_2O) groups. O6 and O8 each refined to complete occupancy which, when allowing for the difference in equipoint rank, contributes 4 (H_2O) groups to the formula unit; O13, O14 and O15 refined to approximately half-occupied: 0.53(3), 0.20(1) and 0.27(1) contributing a total of 2.12 + 0.80 + 1.08 = 4.00 (H_2O) groups to the formula unit. Thus there are 8 (H_2O) groups per formula unit.

The *Cu*2 and *Cu*3 octahedra each form chains of edge-sharing octahedra extending parallel to the b axis (Fig. 4a). The *Cu*1 square pyramid shares two edges with the *Cu*2 octahedron and two corners with the *Cu*3 octahedron, linking the chains of octahedra into a sheet (Figs 4a,b) oriented parallel to {100}. *S*1 and *S*2 tetrahedra decorate the sheet, each sharing one corner with a *Cu* octahedron, and the sheets are held together by interstitial Ce^{3+}, Ca^{2+} and hydrogen bonding (Fig. 4b).

Table 4. Interatomic distances (Å) in bridgesite-(Ce).

*S*1–O4	1.445(13)	*Cu*1–O1 ×2	1.978(8)
*S*1–O7	1.436(15)	*Cu*1–O1 ×2	1.980(9)
*S*1–O12 ×2	1.47(2)	*Cu*1–O4	2.384(12)
<*S*1–O>	1.455	<*Cu*1–O>	2.060
*S*2–O9	1.457(15)	*Cu*2–O1 ×2	1.946(8)
*S*2–O10	1.433(18)	*Cu*2–O5 ×2	1.953(7)
*S*2–O11 ×2	1.448(13)	*Cu*2–O4 ×2	2.522(8)
<*S*2–O>	1.447	<*Cu*2–O>	2.140
Ce–O1 ×2	2.488(8)	*Cu*3–O1 ×2	1.962(7)
Ce–O2 ×2	2.438(9)	*Cu*3–O3 ×2	1.961(7)
Ce–O3	2.501(10)	*Cu*3–O9 ×2	2.587(8)
Ce–O5	2.917(14)	<*Cu*3–O>	2.170
Ce–O6	2.508(13)		
Ce–O11 ×2	2.475(12)	*Ca*–O9	2.82(2)
Ce–O14	2.74(4)	*Ca*–O10	2.388(18)
<*Ce*–O>	2.546	*Ca*–O12 ×2	2.58(2)
		Ca–O13 ×2	2.51(3)
		<*Ca*–O>	2.56

Table 5. Powder diffraction data (*d* in Å) of a bridgesite-(Ce) aggregate measured using micro-X-ray diffraction. The five strongest lines are highlighted in bold.

I	$d_{(meas)}$	*h*	*k*	*l*	*I*	$d_{(meas)}$	*h*	*k*	*l*
100	**11.300**	**2**	**0**	**0**	4	3.081	$\bar{5}$	1	3
3	9.930	$\bar{2}$	0	1	1	3.069	$\bar{8}$	0	2
15	**6.391**	**2**	**0**	**1**	1	3.060	2	2	0
4	6.141	$\bar{4}$	0	1	3	2.952	2	0	3
4	5.646	4	0	0	1	2.853	1	1	3
3	5.136	0	0	2	3	2.830	$\bar{8}$	0	3
1	5.016	1	1	1	2	2.820	$\bar{4}$	0	4
2	4.961	$\bar{4}$	0	2	**8**	**2.770**	**4**	**2**	**0**
5	**4.858**	**3**	**1**	**0**	4	2.708	$\bar{6}$	0	4
3	4.256	4	0	1	2	2.703	0	2	2
3	4.131	$\bar{6}$	0	1	1	2.676	$\bar{4}$	2	2
3	4.124	$\bar{3}$	1	2	1	2.572	$\bar{3}$	1	4
2	3.906	$\bar{6}$	0	2	2	2.568	6	0	2
1	3.735	$\bar{2}$	0	3	1	2.536	7	1	1
4	3.631	$\bar{5}$	1	2	2	2.519	$\bar{6}$	2	1
6	**3.194**	**4**	**0**	**2**	3	2.507	2	2	2
2	3.179	0	2	0					

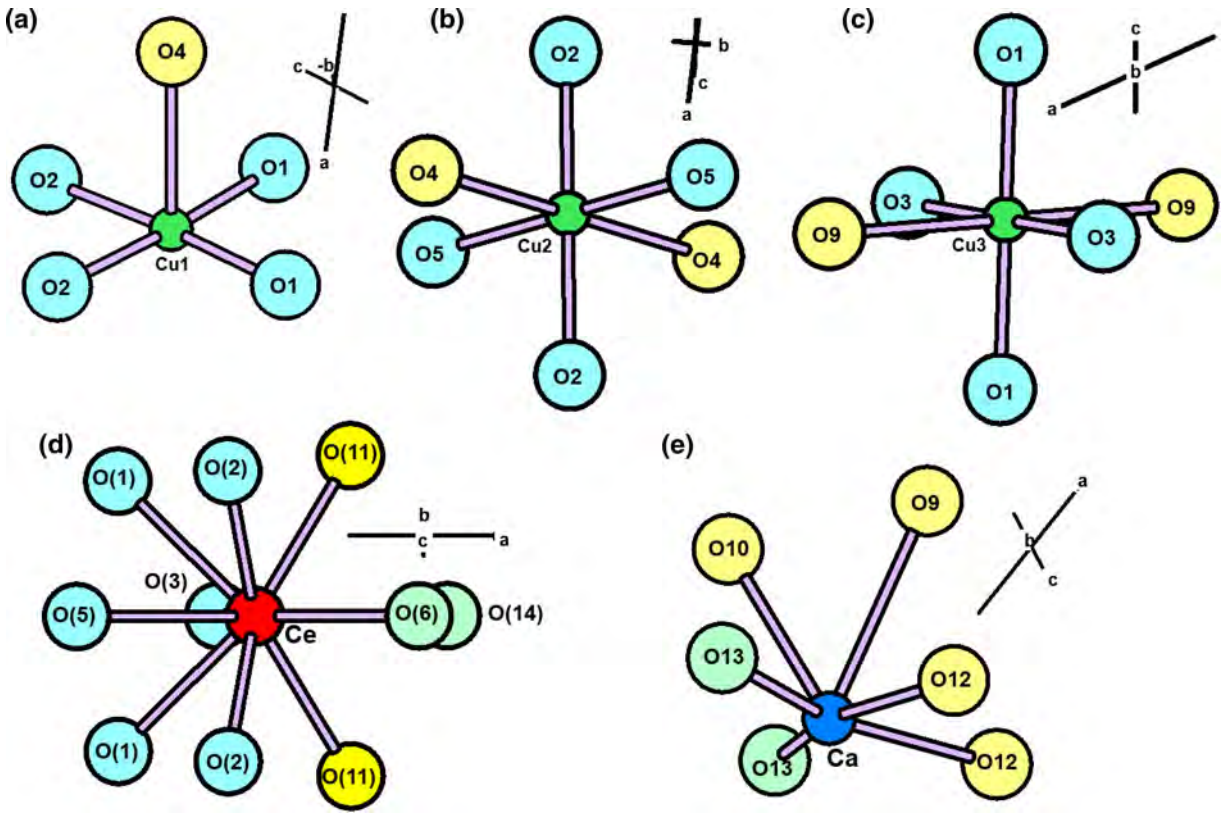

Fig. 3. Coordination polyhedra for the cations in bridgesite-(Ce): (a) Cu1; (b) Cu2; (c) Cu3; (d) Ce; and (e) Ca. Legend: Cu^{2+}: green; Ce^{3+}: red; Ca^{2+}: dark blue; O^{2-}: yellow; $(OH)^{-}$: pale blue; and $(H_2O)^0$: pale green

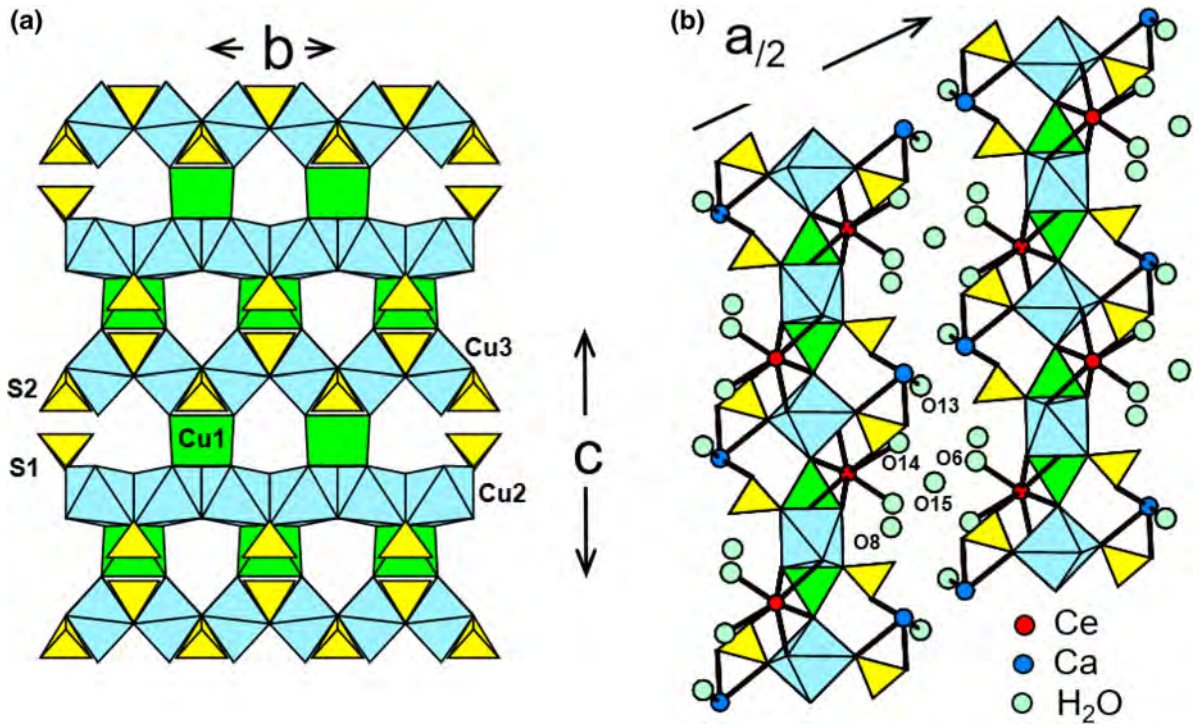

Fig. 4. The crystal structure of bridgesite-(Ce): (a) the $[Cu_3(SO_4)_2(OH)_6]$ sheet; (b) the $[Cu_3(SO_4)_2(OH)_6]$ sheets viewed edge-on, showing the interstitial Ce and Ca. Green: Cu1 square pyramid; blue: Cu2 and Cu3 octahedra; yellow: $(SO_4)^{2-}$ groups; dark-blue circles: Ca; red circles: Ce; and pale green circles: (H_2O) groups.

Table 6. Bond valence* sums for bridgesite-(Ce).

	Ca	Ce	Cu1	Cu2	Cu3	S1	S2	Σ	Assignment
O1		0.38 $^{\times 2\downarrow}$	0.44 $^{\times 2\downarrow}$		0.46 $^{\times 2\downarrow}$			1.28	OH
O2		0.43 $^{\times 2\downarrow}$	0.44 $^{\times 2\downarrow}$	0.48 $^{\times 2\downarrow}$				1.35	OH
O3		0.37			0.46 $^{\times 2\downarrow\rightarrow}$			1.29	OH
O4			0.14	0.10 $^{\times 2\downarrow\rightarrow}$		1.61		1.95	O
O5		0.13		0.47 $^{\times 2\downarrow\rightarrow}$				1.07	OH
O6		0.36						0.36	H_2O
O7						1.64		1.64	O
O8								0	H_2O
O9	0.11				0.08 $^{\times 2\downarrow}$		1.56	1.83	O
O10	0.31						1.65	1.96	O
O11		0.40 $^{\times 2\downarrow}$					1.59 $^{\times 2\downarrow}$	1.99	O
O12	0.19 $^{\times 2\downarrow}$					1.51 $^{\times 2\downarrow}$		1.7	O
O13	0.23 $^{\times 2\downarrow}$							0.23	H_2O
O14		0.2						0.2	H_2O
O15								0	H_2O
Σ	1.26	3.48	1.9	2.1	2	6.27	6.39		

*From Gagné and Hawthorne (2015).

The structure is quite disordered as is apparent from the very weak diffracted intensities above 50°2θ, and several of the atoms have large anisotropic-displacement parameters. It was possible to 'split' some of these atoms and reduce the R_1 index, but this led to the splitting of other bonded atoms to produce unreasonable interatomic distances, and continuation of this process led to instability in the refinement, a result of the lack of high-angle data. Thus we decided to present an average model. The most notable positional disorder involves the O12 O^{2-} ion which has an isotropic-displacement parameter of 0.23 (Table 3). The O12 ion bonds to S^{6+} at the *S*1 site and either Ca^{2+} or vacancy at the half-occupied *Ca* site. Where both S^{6+} and Ca^{2+} bond to O12, the *S*1–O12 bond will be much longer than in the local arrangement where O12 bonds only to S^{6+}. In the latter case, the valence-sum rule requires a significantly shorter (stronger) *S*1–O12 bond than where O12 bonds to Ca^{2+} at the *Ca* site. This variation in *S*1–O12 distance is apparent in the high standard deviation on the *S*1–O12 bond (Table 4) and the large displacement factor at the O12 site (Table 3). The incident bond-valence sum at O7 is low (1.64 vu, Table 6); this is due to the fact that O7 will be an acceptor anion for several hydrogen bonds from the H_2O groups (probably O6 and O13) in the structure.

All the anions bonded to S^{6+} (S1 and S2) are O^{2-} and contribute the 8 O^{2-} to the formula unit; all anions bonded to Cu^{2+} (excluding O4 which is also bonded to S^{6+}) are $(OH)^-$ groups which contribute the 12 $(OH)^-$ to the formula unit. All other ligands are $(H_2O)^0$ groups, for a total of 8 (H_2O) groups per formula unit (see above).

FTIR spectroscopy

A Fourier-transform infrared (FTIR) absorption spectrum was not possible from the holotype specimen due to limited material, therefore a further sample was subsampled. Powdered bridgesite-(Ce) was mixed (~2 wt.%) with dry KBr and a 5 mm diameter disc was manufactured. The disc was analysed using an iS50 FTIR benchtop spectrometer (Thermo Nicolet) with a DTGS KBr detector and a KBr beamsplitter. Spectra were collected in the range 400–4000 cm^{-1} at a resolution of 2 cm^{-1}. A total of 64 scans were collected for each spectrum.

The resultant FTIR spectrum of bridgesite-(Ce) is presented in Fig. 5 for reference purposes. Prominent bands are present between 3000 and 3600 cm^{-1}, corresponding to H_2O and OH (a small peak can be observed at 3410 cm^{-1}), at 1100 cm^{-1}

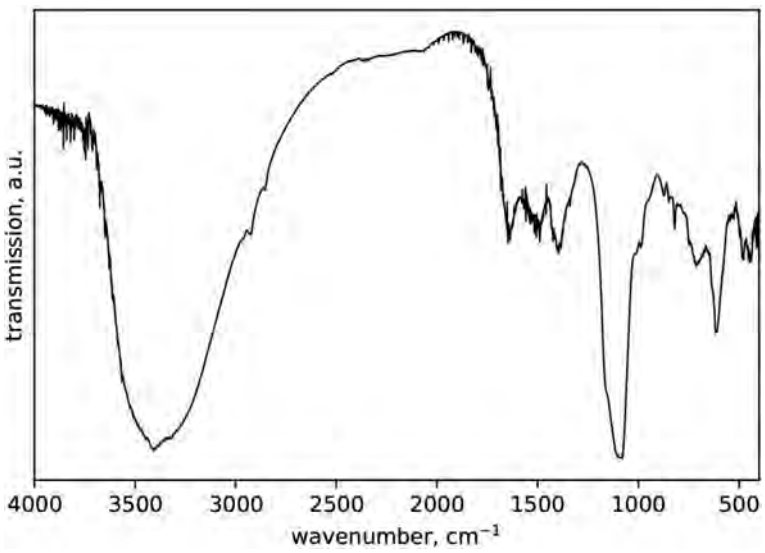

Fig. 5. FTIR absorption spectra of bridgesite-(Ce).

correlating to SO_4 and a region between 550 and 750 cm^{-1}, which is comparable to bands observed in the spectrum of $Ce(SO_4)\cdot 4H_2O$ (Nyquist and Kagel 1971).

Discussion

Bridgesite-(Ce) is a new Cu-sulfate with a unique combination of elements that is not closely related to any of the other Cu-sulfates that have been found in Nature. Despite the similarity of the $(A)Cu_3(SO_4)_2(OH)_6$ part of the reduced formula to the $(A)Cu_4(SO_4)_2(OH)_6$ part of the general formula of the devilline-group minerals, the difference in the number of Cu^{2+} cations means that a continuous sheet of edge-sharing octahedra is not possible in bridgesite-(Ce). Thus the sheet in bridgesite-(Ce), with trigonal–prismatic coordination of one Cu^{2+} ion (Fig. 4) bears no resemblance to the sheet in the devilline group. The visual similarity of bridgesite-(Ce) to members of the devilline group may have precluded its detection and identification before this study, and it is likely to be found elsewhere in the future, indeed after publication in the CNMNC newsletter, a significant number of samples from the same locality have come to light and it is hoped that researchers in the future will be able to use them to improve on the characterisation data presented herein. Bridgesite-(Ce) joins a limited suite of minerals currently identified that contain rare earth elements and the sulfate anion, it is one of the more geochemically simple minerals of this kind.

Acknowledgements. All authors would like to thank Dr David Green for constructive comments regarding the manuscript, Roy Starkey for tracking down an obscure reference and all the reviewers and editors for their comments, suggested improvements, and their time. FCH was supported by a Discovery grant from the Natural Sciences and Engineering Research Council of Canada and by Innovation Grants from the Canada Foundation for Innovation.

Supplementary material. To view supplementary material for this article, please visit https://doi.org/10.1180/mgm.2022.41

References

Bartelmehs K.L., Bloss F.D., Downs R.T. and Birch J.B. (1992) Excalibr II. *Zeitschrift fur Kristallographie*, **199**, 185–196.

Bridges T.F. and Green D.I. (2007). Zoned oxidation deposits in Tynebottom Mine, Garrigill, Cumbria. *Journal of the Russell Society*, **10**, 3–9.

Brown I.D. (2016) *The Chemical Bond in Inorganic Chemistry. The Bond Valence Model. 2nd Edition*. Oxford University Press, UK.

Burns P.C. and Hawthorne F.C. (1996) Static and dynamic Jahn-Teller effects in Cu^{2+}-oxysalt minerals. *The Canadian Mineralogist*, **34**, 1089–1105.

Dunham K.C. (1948) *Geology of the Northern Pennine Orefield*. British Geological Survey, Keyworth, UK, pp. 357.

Eby R.K. and Hawthorne F.C. (1993) Structural relations in copper oxysalt minerals. I. Structural hierarchy. *Acta Crystallographica*, **B49**, 28–56.

Gagné O.C. (2018) Bond-length distributions for ions bonded to oxygen: results for the lanthanides and actinides and discussion of the f-block contraction. *Acta Crystallographica*, **B74**, 49–62.

Gagné O.C. and Hawthorne F.C. (2015) Comprehensive derivation of bond-valence parameters for ion pairs involving oxygen. *Acta Crystallographica* **B71**, 562–578.

Gagné O.C. and Hawthorne F.C. (2018) Bond-length distributions for ions bonded to oxygen: Results for the non-metals and discussion of lone-pair stereoactivity and the polymerization of PO_4. *Acta Crystallographica*, **B74**, 79–96.

Hawthorne F.C. (2012) A bond-topological approach to theoretical mineralogy: crystal structure, chemical composition and chemical reactions. *Physics and Chemistry of Minerals*, **39**, 841–874.

Hawthorne F.C. (2015) Toward theoretical mineralogy: a bond-topological approach. *American Mineralogist*, **100**, 696–713.

Hawthorne F.C., Krivovichev S.V. and Burns P.C. (2000) The crystal chemistry of sulfate minerals. Pp. 1–112 in: *Sulfate Minerals: Crystallography, Geochemistry and Environmental Significance* (C.N. Alpers, J.L. Jambor and D.K. Nordstrom, editors). Reviews in Mineralogy and Geochemistry, **40**. Mineralogical Society of America, Washington DC.

Ixer R.A. (2003), The distribution of rare earth elements in north Pennine fluorspar and fluorite. *UK Journal of Mines and Minerals*, **23**, 21–26.

Ixer R.A. and Stanley C.J. (1987). A silver-nickel-cobalt mineralisation at Tynebottom mine, Garrigill, near Alston, Cumbria. *Proceedings of the Yorkshire Geological Society*, **46**, 133–139.

Mandarino J.A. (2007) The Gladstone–Dale compatibility of minerals and its use in selecting mineral species for further study. *The Canadian Mineralogist*, **45**, 1307–1324.

Nyquist R.A. and Kagel R.O. (1971) *Infrared Spectra of Inorganic Compounds*. Academic Press, New York.

Rumsey M.S., Hawthorne F. and Spratt J. (2019) Bridgesite-(Ce), IMA 2019-034. CNMNC Newsletter No. 52. *Mineralogical Magazine*, **83**, 887–893.

Sheldrick G.M. (2008) A short history of SHELX. *Acta Crystallographica*, **A64**, 112–122.